

# Nanoscale

Accepted Manuscript



This is an *Accepted Manuscript*, which has been through the Royal Society of Chemistry peer review process and has been accepted for publication.

*Accepted Manuscripts* are published online shortly after acceptance, before technical editing, formatting and proof reading. Using this free service, authors can make their results available to the community, in citable form, before we publish the edited article. We will replace this *Accepted Manuscript* with the edited and formatted *Advance Article* as soon as it is available.

You can find more information about *Accepted Manuscripts* in the [Information for Authors](#).

Please note that technical editing may introduce minor changes to the text and/or graphics, which may alter content. The journal's standard [Terms & Conditions](#) and the [Ethical guidelines](#) still apply. In no event shall the Royal Society of Chemistry be held responsible for any errors or omissions in this *Accepted Manuscript* or any consequences arising from the use of any information it contains.

## ARTICLE

# Biotin-decorated silica coated PbS nanocrystals emitting in the second biological near infrared window for bioimaging

Cite this: DOI: 10.1039/x0xx00000x

Received 00th January 2012,  
Accepted 00th January 2012

DOI: 10.1039/x0xx00000x

[www.rsc.org/](http://www.rsc.org/)M. Corricelli,<sup>†,a,b</sup> N. Depalo,<sup>†,b</sup> E. Di Carlo,<sup>a</sup> E. Fanizza,<sup>a,b</sup> V. Laquintana,<sup>c</sup> N. Denora,<sup>c</sup> A. Agostiano,<sup>a,b</sup> M. Striccoli,<sup>b</sup> M. L. Curri,<sup>\*,b</sup>

Nanoparticles (NPs) emitting in the second biological near infrared (NIR) window of the electromagnetic spectrum have been successfully synthesized by growing a silica shell onto the hydrophobic surface of OLEA/TOP PbS nanocrystals (NCs), by means of reverse microemulsion approach, and subsequently decorated with biotin molecules. The fabrication of very uniform and monodisperse NPs formed of SiO<sub>2</sub> shell coated single core PbS NCs, has been demonstrated by means of a set of complementary optical and structural techniques (Vis-NIR Absorption and Photoluminescence Spectroscopy, Transmission Electron Microscopy) that have highlighted how experimental parameters, such as PbS NC and silica precursor concentration, are crucial to direct morphology and optical properties of silica coated PbS NPs. Subsequently, the silica surface of the core shell NPs has been grafted with amino groups, in order to achieve covalent binding of biotin to NIR emitting silica coated NPs. Finally the successful reaction with a green-fluorescent labelled streptavidin has verified the molecular recognition response of the biotin molecules decorating the PbS@SiO<sub>2</sub> NP surface. Dynamic light scattering (DLS) and ζ-potential techniques have been used to monitor hydrodynamic diameter and colloidal stability of both PbS@SiO<sub>2</sub> and biotin decorated NPs, showing their high colloidal stability in physiological media, as needed for biomedical applications. Remarkably the obtained biotinylated PbS@SiO<sub>2</sub> NPs have been found to retain emission properties in the 'second optical window' of NIR region of electromagnetic spectrum, thus representing attractive receptor-targeted NIR fluorescent probes for in vivo tumour imaging.

## Introduction

Near infrared (NIR) emitting semiconductor nanocrystals (NCs) are emerging as revolutionary labelling materials for in vivo and deep-tissue imaging of biological targets, due to the unmatched tunability in their optical properties. In the first (700 - 900 nm) and second (1000 - 1400 nm) optical window of the NIR region of the electromagnetic spectrum, the light attenuation by the absorption and scattering from the main tissue constituents (water, lipid, haemoglobin, melanin) is significantly reduced, thus allowing luminescent probes which operate at these wavelengths to penetrate biological systems very deeply, down to millimetres and even centimetres scale. Interestingly, optical simulations have recently proved that the use of NCs emitting in the 'second optical window' can improve the imaging sensitivity up to about 100 times.<sup>1-5</sup> Although several types of NIR-emitting NCs have been developed for bioimaging, the synthesis of non-toxic and biocompatible nanoparticles (NPs) emitting in the NIR region,

and in particular in the 'second biological window' (1000 - 1400 nm), remains still a challenge.<sup>6</sup> In fact, most semiconductor nanomaterials such as PbSe, PbS and CdHgTe NCs, which are promising candidate for imaging in the 'second biological window', are based on toxic elements, thus resulting unsuitable to use them for in vivo imaging. In this perspective, among the different approaches to develop safe systems, the growth of a silica shell on the NC surface represents an efficient and widely accepted method to prevent NC toxicity and to impart them biocompatibility. Indeed, the surface coating of colloidal NCs with an inert silica layer results in robust and water soluble core-shell nanostructures, which are able to preserve the NC optical properties.<sup>7</sup> Moreover a silica shell offers a versatile platform for chemical modification with convenient functional groups for subsequent decoration with biomolecules, thus yielding original multifunctional hybrid nanoarchitectures with a great potential for biomolecular therapeutics and biomedicine.<sup>8-10</sup>

Many applications of PbS NCs in the area of optoelectronics have been reported in literature, as PbS is an important semiconducting material with a narrow band gap energy and a large Bohr radius of 18 nm,<sup>11-15</sup> which make this material also a good candidate for fibre-optic communication systems, being the telecommunication band defined in the range 1200 - 1700 nm.<sup>16</sup> On the contrary, only very few studies on the use of PbS NCs for optical bioimaging have been so far carried out.<sup>17,18</sup> For example, polyethylene glycol (PEG) modified phospholipid micelles encapsulating PbS NCs have been conjugated with folic acid and used to targeted imaging of pancreatic cancer cells.<sup>19</sup> Moreover, silica coated PbS NPs have been functionalized with a PEG-phospholipid dual layer and successfully applied for in vivo sentinel lymph node mapping of mice.<sup>20</sup> In the both cases, PbS NCs emitting in the 'first optical window' have been studied, while examples of PbS NCs emitting in the 'second optical window' have not been reported, so far.

Here, for the first time, the synthesis of uniform and monodisperse core-shell structures formed of silica coated PbS NCs emitting in the 'second biological window' has been successfully realized. In addition, bio-conjugation with activated biotin has been subsequently carried out in order to fabricate target-specific NPs, thus demonstrating their ability to covalently bind at the surface of the silica coated PbS NCs, biomolecules which can be used for applications in biomedical field.

The growth of a silica shell on the hydrophobic OLEA/TOP-capped PbS NC surface, by means of a water-in-oil reverse microemulsion approach, has been fully investigated, by using different spectroscopic and structural techniques, as a function of several experimental parameters, such as PbS NC, silica precursor and ammonia solution concentration. Interestingly, a strong dependence of the optical properties on the final NP morphology has been found. The surface of the silica coated NPs has been further functionalized with amino groups, essential for coupling them to the organic moiety, for the ultimate fabrication of complex and multifunctional biologically relevant nanostructures.

Biotin decorated silica coated PbS NPs have been prepared by means of a bio-conjugation reaction between amino groups and activated biotin. The success of the biotinylation process has been assessed by means of a molecular recognition reaction with a green-fluorescent FITC-labelled avidin protein. Biotin, a growth promoter of cells, is one of the most common tumour recognition moieties, since its content in cancerous tumour is significantly higher than in normal tissue. The rapid proliferation of cancer cells requires extra biotin, and such cancer cells often over-express biotin specific receptors on the cell surface. The specific interaction between biotin and its receptors may be explored for specific tumour cell targeting.<sup>21,22</sup> In our work the biotinylated silica coated PbS NPs retained emission properties in the 'second optical window', thus representing attractive receptor-targeted NIR fluorescent probes for in vivo tumour imaging.

## Experimental

### Materials

Lead(II) oxide (PbO, powder 99.99%), hexamethyldisilathiane (HMDS, synthesis grade), 1-octadecene (ODE, 90% technical grade, Sigma-Aldrich), oleic acid (OLEA, technical grade 90%, Sigma-Aldrich), trioctylphosphine (TOP, 90% technical grade), aqueous ammonia (NH<sub>4</sub>OH, 28-30% H<sub>2</sub>O), tetraethyl orthosilicate (TEOS, 98%), polyoxyethylene (5) nonylphenylether branched (Igepal CO-520), 3-aminopropyltriethoxysilane (APS, 97%), Biotin N-hydroxysuccinimide ester ( $\geq 98\%$ ), Streptavidin-FITC from Streptomyces avidinii ( $\geq 5$  units/mg protein) and aqueous ammonia (d=0.900 g/mL, NH<sub>4</sub>OH) were purchased by Sigma-Aldrich and used as received. All solvents, namely ethanol, chloroform, cyclohexane, tetrachloroethylene (TCE), dimethylsulfoxide (DMSO), also purchased by Sigma-Aldrich, are of the highest purity available. All aqueous solutions have been prepared by using water obtained by Milli-Q Gradient A-10 system (Millipore, 18.2 M $\Omega$  cm, organic carbon content  $4 \leq \mu\text{g/L}$ ).

### Synthesis of PbS Nanocrystals

PbS NCs have been synthesized as previously reported by Corricelli et al.<sup>23</sup> In a typical synthesis, 4 mmol of PbO, 9.0 mL of trioctylphosphine (TOP), and 2.7 mL of oleic acid (OLEA) have been added in a three-neck flask containing 36 mL of 1-octadecene (ODE). The reaction mixture has been left stirring under vacuum at 120 °C; at this stage the formation of lead-oleate precursors occurred. Subsequently, a 20 mM solution of the sulphur precursor, hexamethyldisilathiane (HMDS) in ODE, with a Pb/S molar ratio of 2:1, has been swiftly injected. The temperature has been suddenly cooled to 80 °C in order to prevent further nucleation and promote the growth of the freshly formed nuclei. The reaction has been stopped after 13 minutes and PbS NCs have been then collected by centrifugation after the addition of ethanol, as non-solvent. Three centrifugation steps were required to ensure the complete removal of OLEA excess, as well as unreacted precursors. The PbS NCs, recovered as a black powder, have been then dispersed in toluene.

### Silica coating of PbS nanocrystals

Silica shell has been grown on PbS NC surface exploiting a water in oil (W/O) microemulsion approach<sup>24,25</sup> investigating the influence of PbS NC, ammonia and TEOS concentration on the morphology of the final shell. Four different concentrations of PbS NCs dispersed in cyclohexane, prepared after removal of the original solvent (toluene), have been tested (namely,  $2.5 \cdot 10^{-6}$  M,  $6.1 \cdot 10^{-6}$  M,  $9.5 \cdot 10^{-6}$  M and  $1.2 \cdot 10^{-5}$  M). Then, Igepal CO-520 (700  $\mu\text{L}$ ), ammonia solution (350  $\mu\text{L}$ , 400  $\mu\text{L}$ , 520  $\mu\text{L}$  and 600  $\mu\text{L}$ ) and TEOS (25  $\mu\text{L}$ , 30  $\mu\text{L}$  and 80  $\mu\text{L}$ ), in this sequence, have been added, to cyclohexane PbS NC solution (12 mL). The obtained reverse microemulsion has been kept for 20 hours at 28°C under vigorous stirring. Subsequently, the

disruption of reverse microemulsion has been achieved by addition of methanol (~10 mL) to the reaction mixture and the silica coated PbS NCs have been then collected by centrifugation and washed twice with ethanol (15 mL). Finally, the PbS@SiO<sub>2</sub> NPs have been dispersed in the minimum volume of ethanol (2 mL).

#### **PbS@SiO<sub>2</sub> nanoparticle functionalization with primary amine groups**

In a three-neck flask, 2 mL of a PbS@SiO<sub>2</sub> NP solution (1.4·10<sup>14</sup> part/mL), 7 mL of ethanol and 1 mL of APS solution in ethanol (0.29 M) have been mixed under vigorous stirring for 2 hours, at room temperature. Subsequently, the temperature has been increased up to 80°C, and the reaction mixture has been kept at this temperature for 1 hour. In the first step, the formation of hydrogen bonds between hydroxyl groups on PbS@SiO<sub>2</sub> NPs and in APS molecules occurred; the covalent binding has been then induced by the heating, resulting in a concomitant release of water molecules. After cooling at room temperature, the amine functionalized PbS@SiO<sub>2</sub> NPs have been purified by repeated cycles of centrifugation and dispersion in ethanol. Finally, the collected NPs have been dispersed in 1.5 mL of a H<sub>2</sub>O:DMSO mixture (1:1).

#### **Biotinylation of amine functionalized PbS@SiO<sub>2</sub> nanoparticles**

Biotin N-hydroxysuccinimide ester in DMSO (2 mL, 0.06 M) has been mixed with 1 mL of the solution containing amine functionalized PbS@SiO<sub>2</sub> NPs dispersed in H<sub>2</sub>O:DMSO=1:1 (1.9·10<sup>14</sup> part/mL), under vigorous stirring for 2 hours, at room temperature. The biotinylated PbS@SiO<sub>2</sub> NPs have been then purified, centrifuging and washing with DMSO (four times). Finally, the biotin decorated NPs have been dispersed in 2 mL of sodium bicarbonate buffer (25 mM, pH=9.5).<sup>26</sup>

#### **Molecular recognition reaction of biotinylated PbS@SiO<sub>2</sub> nanoparticles with FITC-streptavidin**

FITC-labeled streptavidin solution (1 mL) at concentration of 1 mg/mL in sodium bicarbonate buffer (25 mM, pH=9.5) has been added to 1 mL of biotinylated PbS@SiO<sub>2</sub> NPs (1.0·10<sup>14</sup> part/mL), prepared as previously described, under vigorous magnetic stirring for 2 hours, in the dark. This procedure has been followed in order to promote the interaction between biotin and streptavidin moieties. After incubation, the reaction mixture has been centrifuged and the recovered precipitate has been washed (four times) with sodium bicarbonate buffer (25 mM, pH=9.5), in order to remove the excess of free FITC-streptavidin. The biotinylated PbS@SiO<sub>2</sub> NPs conjugated with fluorescent streptavidin have been dispersed in 1 mL of bicarbonate buffer (25 mM, pH=9.5).

#### **Vis-NIR absorption and emission characterization of nanoparticles**

Vis-NIR absorption spectra have been acquired using optically coupled quartz cuvettes (optical length=1 mm), firstly recording

the baseline (solvent vs solvent) and, successively, the sample spectrum (sample vs solvent), in order to minimize the solvent absorption in the zone of interest. A Cary Varian 5000 UV-visible-NIR spectrophotometer has been used. PL emission measurements have been performed with a Horiba Jobin Yvon Fluorolog-3 spectrofluorimeter, using a 450 Xe lamp as excitation source, coupled to a double grating Czerny-Turner monochromator for wavelength selection. The detection system consists of a TBX-PS detector in the visible range and a Peltier-cooled InGaAs detector in the NIR range.

#### **Structural characterization of the nanoparticles**

Transmission Electron Microscopy (TEM) analysis has been performed by using a Jeol Jem-1011 microscope, working at an accelerating voltage of 100 kV. TEM images have been acquired by a Quemesa Olympus CCD 11 Mp Camera. The samples have been prepared by dipping the 300 mesh amorphous carbon-coated Cu grid in a PbS NC toluene dispersion or, alternatively in a PbS@SiO<sub>2</sub> NP ethanol dispersion, and letting the solvent to evaporate. Size statistical analysis (NP average size and size distribution) of the samples has been performed by means of freeware Image J analysis program. In particular the average NP size and the percentage relative standard deviation ( $\sigma\%$ ) have been calculated for each sample, to define NP size distribution.

#### **Particle size, size distribution and colloidal stability**

Size, size distribution and colloidal stability of the PbS@SiO<sub>2</sub> NPs have been detected using a Zetasizer Nano ZS, Malvern Instruments Ltd., Worcestershire, UK (DTS 5.00). In particular, NP size and size distribution have been determined by means of dynamic light scattering (DLS). Size distribution is described in terms of polydispersity index (PDI). The  $\zeta$ -potential measurements have been carried out by using a laser Doppler velocimetry (LDV) after sample dilution in KCl aqueous solution (1 mM).

#### **Results and discussion**

NIR emitting and hydrophobic PbS NCs have been synthesized by hot injection technique, yielding highly crystalline NPs with a narrow size-distribution. The growth of a silica (SiO<sub>2</sub>) shell on PbS NC surface has been, then, achieved by means of a water-in-oil microemulsion approach, resulting in NPs with high stability in polar solvent. Biotin decorated silica coated NPs have been prepared by grafting the silica coated NP surface with primary amine groups, followed by reaction with biotin N-hydroxysuccinimide ester (N-biotin). The ability of the biotin to bind the streptavidin has been assessed by promoting a molecular recognition reaction with a green-emitting FITC-modified streptavidin. A scheme depicting the steps which finally led to the bioconjugated NIR-emitting NPs has been reported in Figure 1.

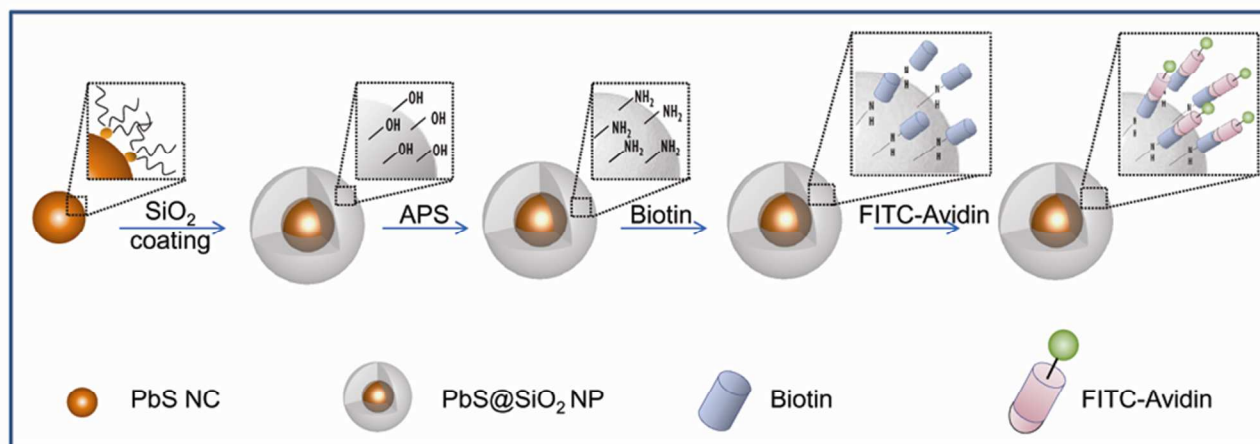


**Figure 1.** General scheme for the PbS NC functionalization process leading to conjugation of PbS@SiO<sub>2</sub> NPs with biotin and their subsequent conjugation with streptavidin. Successive steps in sequence (from left to right): silica coating of organic capped PbS NCs; PbS@SiO<sub>2</sub> NP surface modification with amine groups; bioconjugation reaction with biotin; molecular recognition with FITC-modified streptavidin.

### Structural and spectroscopic characterization of organic coated PbS nanocrystals

The as-prepared organic capped PbS NCs have been characterized by optical absorption and emission spectroscopy, as well as TEM measurements. Interestingly, a well-resolved excitonic transition signal, at 1026 nm, can be clearly observed in the absorption spectrum of the PbS NCs dispersed in toluene (Figure 2a, black line). In addition, their photoluminescence emission spectrum is characterized by the presence of a single narrow emission peak, hence in the ‘second biological window’ of the electromagnetic spectrum, with a Stoke shift of 109 nm with respect to the corresponding absorption band (Figure 2a, red line). Such an emission peak can be ascribed to band-edge recombination, whereas no signal can be ascribed to defect states. The structural characterization carried out by means of TEM and HRTEM investigation has revealed the high crystalline quality of the NCs, with a narrow size-distribution, as also confirmed by the corresponding size distribution histogram (Figure 2b and S1). In particular, the average diameter of PbS NCs obtained by the statistical analysis is of  $3.0 \pm 0.6$  nm.

### Growth of a silica shell on the PbS nanocrystals

The growth of the silica shell on PbS NC surface has been carried out by means of a reverse W/O microemulsion approach.<sup>24,25</sup> Namely, the proper amounts of Igepal CO-520, ammonia aqueous solution and TEOS have been swiftly injected, at 28°C, in a cyclohexane dispersion of PbS NCs at defined concentration. At this stage the solution appears slightly turbid until the ternary system reaches an equilibrium, allowing the water droplet incorporation in the reverse micelles, while PbS NCs are still localized in the organic phase. The reaction proceeds via encapsulation of quickly hydrolysed

TEOS molecule in the aqueous droplets. Subsequently, the pristine capping ligands (OLEA/TOP) coordinating PbS NC surface, are replaced by TEOS molecules at the water/oil interface, allowing the PbS NC inclusion in the aqueous core of the reverse micelles. At this point, both the nucleation and the growth of silica on PbS NC surface occur in the confined geometry of the aqueous droplets, which acts as a nanoreactor and defines the final size and shape of the silica beads.<sup>27,28</sup> Interestingly, the relative Igepal/ammonia molar ratio determines the number and size of the reverse micelles.<sup>29-31</sup> As previously experimentally observed, when the number of NCs matches the number of micelles, almost all the micelles are occupied by one NC, resulting in a high yield of core-shell nanostructures. Conversely, lower NC concentration results in a lower occupancy degree of micelles, thus inducing the formation of bare silica beads. On the contrary, higher NC concentration promotes the incorporation of multiple NC cores in a single silica bead. The influence of PbS NC concentration, as well as of ammonia solution and TEOS volume, respectively, on the final morphology and optical properties of silica coated PbS NCs, has been here investigated.

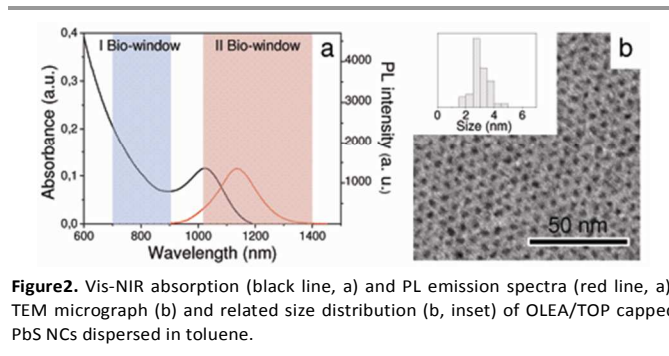


**Figure 2.** Vis-NIR absorption (black line, a) and PL emission spectra (red line, a), TEM micrograph (b) and related size distribution (b, inset) of OLEA/TOP capped PbS NCs dispersed in toluene.

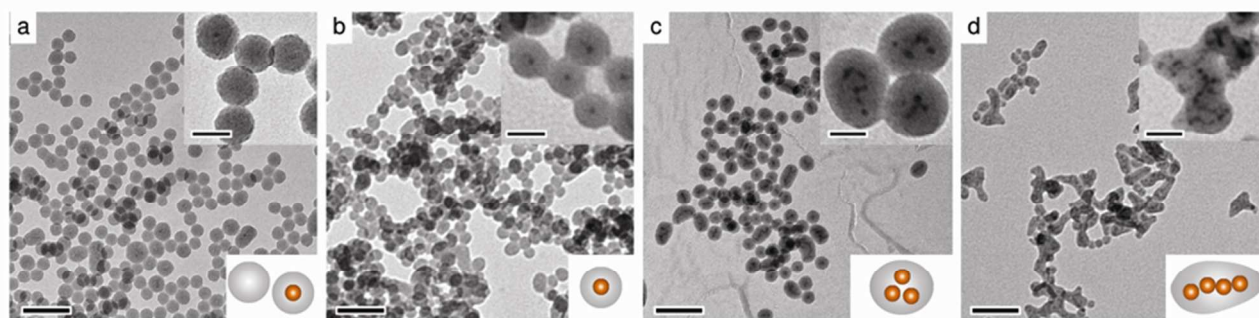


**Figure 3.** TEM micrographs of PbS@SiO<sub>2</sub> nanostructures, at different magnification (scale bar = 100 nm and 25 nm, respectively), prepared keeping the volume of Igepal (700  $\mu$ L), ammonia (400  $\mu$ L) and TEOS (30  $\mu$ L) constant and varying PbS NC concentrations:  $2.5 \cdot 10^{-6}$  M (a),  $6.1 \cdot 10^{-6}$  M (b),  $9.5 \cdot 10^{-6}$  M (c) and  $1.2 \cdot 10^{-5}$  M (d).

Keeping constant the volume of Igepal, ammonia solution and TEOS at 700  $\mu$ L, 400  $\mu$ L and 30  $\mu$ L, respectively, different morphology of the silica nanostructures have been obtained. While a variable multiplicity of PbS NCs embedded in a single silica bead has been observed by increasing the PbS NC concentrations ( $2.5 \cdot 10^{-6}$  M,  $6.1 \cdot 10^{-6}$  M,  $9.5 \cdot 10^{-6}$  M and  $1.2 \cdot 10^{-5}$  M), as shown by TEM micrographs in Figure 3. In particular, when PbS NC concentration is equal to  $2.5 \cdot 10^{-6}$  M, beads with a regular spherical shape have been obtained (Figure 3a). However, carefully looking at the inset of Figure 3a, two different kinds of particles are clearly observable, namely bare, "empty", silica NPs and core-shell PbS@SiO<sub>2</sub> NPs. Spherical core shell structures with an average diameter of  $27 \pm 4$  nm and a narrow size distribution ( $\sigma_{\%} = 15\%$ , Figure S2a) have been achieved at PbS NC concentration of  $6.1 \cdot 10^{-6}$  M (Figure 3b). Interestingly, no bare silica NPs have been observed and the presence of cores of about 3 nm can be clearly detected (Inset of Figure 3b), highlighting that a single PbS NC has been incorporated in each silica nanostructure. Hence, it has been possible to estimate the silica shell thickness, obtaining a value of about 11 nm. Increasing PbS NC concentration up to  $9.5 \cdot 10^{-6}$  M, mainly spherical nanostructures with multiple PbS NC cores, ranging from 3 to 7, have been achieved, although elongated silica structures have been also observed (Figure 3c). In this case, the statistical analysis have revealed a larger average diameter ( $31 \pm 5$  nm) and higher polydispersity value ( $\sigma_{\%} = 18\%$ , Figure 2b). Conversely, significant changes in the nanostructure morphology have been found when the tested PbS NC concentration has been further increased up to  $1.2 \cdot 10^{-5}$  M. In particular, a variety of very irregular and interconnected nanostructures with tubular shape and containing very large aggregates of PbS NC cores, has been achieved (Figure 3d). It is thus evident that, when the size and number of the aqueous domains, which are only dependent on the ratio of ammonia to Igepal, remain unchanged, the PbS NC concentration strongly affects the final size and shape of silica coated NPs. High yield of core shell structures, without bare silica NPs, can be obtained only when the amount of PbS NCs is comparable to the micellar population. Therefore, PbS NC concentration of  $6.1 \cdot 10^{-6}$  M is reasonable to ensure the full occupancy of each micelle with one PbS NC, resulting in the most suitable concentration value to match the micellar population, under the

investigated conditions. Decreasing PbS NC concentration down to  $2.5 \cdot 10^{-6}$  M, the number of PbS NCs is insufficient to fill each micellar domain, thus bringing to the formation of "empty" silica beads. On the contrary, an increase in PbS NC concentration leads to more PbS NCs embedded in the same reverse micelle, thus originating nanostructures with multiple NC cores. In addition, the distinct morphology and larger size of such multiple core nanostructures can be accounted by the structural perturbations, occurring in the micellar volume and/or at the interfacial area, which may be experienced by the ternary system based on water/oil/surfactant, due to the addition of small amounts of a solute. The insertion of solute in water pool has been reported to induce an increase of the micellar volume, proportional to the volume of the solute added.<sup>32</sup> Interestingly, the variation of the micellar volume concomitant to the addition of a hydrophilic solute is equivalent to the analogous perturbation observed upon addition of the same volume of water. In addition, in surfactant systems containing large amounts of oil and/or water, the shape and size of surfactant based templates change, with the possible formation of elongated micelles, interconnected channels or cylinders.<sup>32,33</sup> In the investigated case, before the reaction takes place, the presence of PbS NCs in cyclohexane phase still does not perturb the characteristic radius of the micelles. Subsequently, the reaction proceeds by the exchange of the surfactant molecules (OLEA/TOP) on the PbS NC surface with hydrolysed TEOS, at the water/oil interface, prior to NC incorporation in the aqueous domain. At this stage, the PbS NCs act as a solute added into the water pool. If the volume occupied by the solute is not negligible with respect to the micellar volume, the latter will increase as a consequence of the addition of such a solute. The addition of PbS NCs, at concentration values higher than  $6.1 \cdot 10^{-6}$  M in the reverse microemulsion, induces the inclusion of multiple NCs, which produces a change in the micellar volume, finally resulting in larger silica coated NPs. Reasonably, the alteration of micellar volume is more significant when the PbS NC concentration is high ( $1.2 \cdot 10^{-5}$  M), and causes the formation of interconnected cylinders as synthetic template for the silica particles, ultimately resulting in the very irregular silica coated nanostructures.

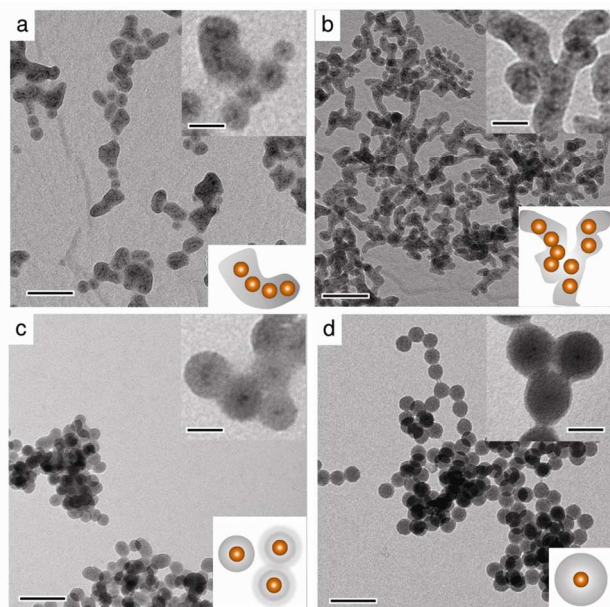


**Figure 4.** TEM micrographs of PbS@SiO<sub>2</sub> NPs, at different magnification (scale bar = 100 nm and 25 nm, respectively), prepared keeping constant the PbS NC concentration ( $6.1 \cdot 10^{-6}$  M) and the volume of Igepal (700  $\mu$ L) and TEOS (30  $\mu$ L) and exploiting the volume of ammonia equal to 520  $\mu$ L (a) and 600  $\mu$ L (b). TEM micrographs of PbS@SiO<sub>2</sub> NPs, at different magnification (scale bar = 100 nm and 25 nm, respectively), prepared keeping constant the PbS NC concentration ( $6.1 \cdot 10^{-6}$  M) and the volume of Igepal (700  $\mu$ L) and ammonia (400  $\mu$ L) and adding a volume of TEOS equal to 25  $\mu$ L (c) and 80  $\mu$ L (d), respectively.

In addition, consequently to the replacement of the pristine capping agents on PbS NC surface, with hydrolysed TEOS molecules, the release of OLEA and TOP molecules in solution can be reasonably assumed. While an amount of these molecules can be supposed to form empty reverse micelles in the organic (cyclohexane) phase, other will organize at the water/oil interphase, intercalating IGEPAL molecules. In this new configuration, a further modification of the ternary system composition, and hence structure, can still occur, finally resulting in the experimentally observed elongated structures.<sup>32,33</sup> Further evidence of this phenomenon has been provided by the observation of very similar morphology for the silica coated nanostructures obtained by increasing the content of the aqueous ammonia solution at values equal to 520  $\mu$ L and 600  $\mu$ L (Figure 4a and b, respectively), while PbS NC concentration has been set at the value of  $6.1 \cdot 10^{-6}$  M. The injected volumes of Igepal and TEOS have been left unchanged at 700  $\mu$ L and 30  $\mu$ L, respectively.

Obviously, the formation of interconnected water channel in the reverse microemulsion takes place also under these conditions, with an increasingly branched morphology, due to the addition of a higher amount of water, resulting in very irregular silica coated nanostructures with a large number of PbS NC cores.<sup>33</sup> Interestingly, when a lower amount of ammonia has been added (350  $\mu$ L), keeping all the other parameters fixed as in the previous cases, the reaction does not take place (data not reported). Probably, in this case, the water content is too low to stabilize the ternary microemulsive system and consequently to

produce the reverse micellar population. Finally, the silica shell growth has been also carried out by keeping constant the microemulsion composition, i.e. volume of IGEPAL (700  $\mu$ L), ammonia solution (400  $\mu$ L) and PbS NC concentration ( $6.1 \cdot 10^{-6}$  M) and increasing the volume of injected TEOS. Previously, it has been demonstrated that the injection of 30  $\mu$ L of TEOS produced regular PbS@SiO<sub>2</sub> NPs, with one PbS NC core and a shell thickness of about 11 nm (Figure 4b). Decreasing the volume of added TEOS to 25  $\mu$ L, a silica shell with a morphology not dissimilar from the case of addition of 30  $\mu$ L of TEOS has been obtained.

However in this case, the silica shell appears inhomogeneous and not well defined, probably due to the insufficient amount of added TEOS which results not enough to ensure a complete silica coverage of the PbS NC surface (Figure 4c). On the other hand, the TEM micrographs (Figure 4d) and the statistical analysis (Figure 2c) of the sample prepared when TEOS volume is increased to 80  $\mu$ L have revealed the formation of spherical and very homogeneous PbS@SiO<sub>2</sub> NPs with a larger average diameter of  $33 \pm 2$  nm and a very narrow size distribution ( $\sigma_{\%} = 6\%$ , Figure 2c). In addition, the observed core-shell structures have revealed one NC core per silica beads, and a thicker shell, of about 15 nm, without any "empty" silica NPs. TEM micrographs of two samples of PbS@SiO<sub>2</sub> NPs, prepared at the same microemulsion composition and at TEOS content of 30  $\mu$ L and 80  $\mu$ L respectively, reported in the inset of Figure 5a and Figure 5b, clearly highlight that, in both cases, regular shape and the very narrow size-distribution that can be achieved. Being the volumes of Igepal and ammonia the same for the both cases, it is evident that the number and size of nanodroplets is identical for these two samples. However, the different amount of TEOS has clearly resulted in different shell thicknesses for the obtained PbS@SiO<sub>2</sub> NPs, thus unambiguously indicating that the silanoic precursor concentration allows to effectively control the silica shell thickness. As previously reported,<sup>34,35</sup> the silica bead formation can be qualitatively explained by means of LaMer theory, typically accounting for growth of amorphous particles. According to this mechanism, the first stage of the process is the TEOS hydrolysis, which causes the formation of the monomers. When the supersaturation condition arises, the heterogeneous nucleation of silica on PbS NC surface occurs. The subsequent growth of silica determines a progressive reduction of the monomer concentration. However, it is well known that the energy barrier for the homogeneous nucleation is lower than the energy required for the heterogeneous nucleation. Indeed, when the monomer concentration is too high and, particularly, is above the threshold for the homogeneous nucleation, core-free SiO<sub>2</sub> particles will be produced and coexist with PbS@SiO<sub>2</sub> NPs. In our case, as the TEM micrographs clearly indicate, the presence of core-free SiO<sub>2</sub> NPs can be excluded, thus meaning that the modulation of TEOS content has been carried out in a concentration range between the critical concentration values for heterogeneous and homogeneous nucleation, respectively.

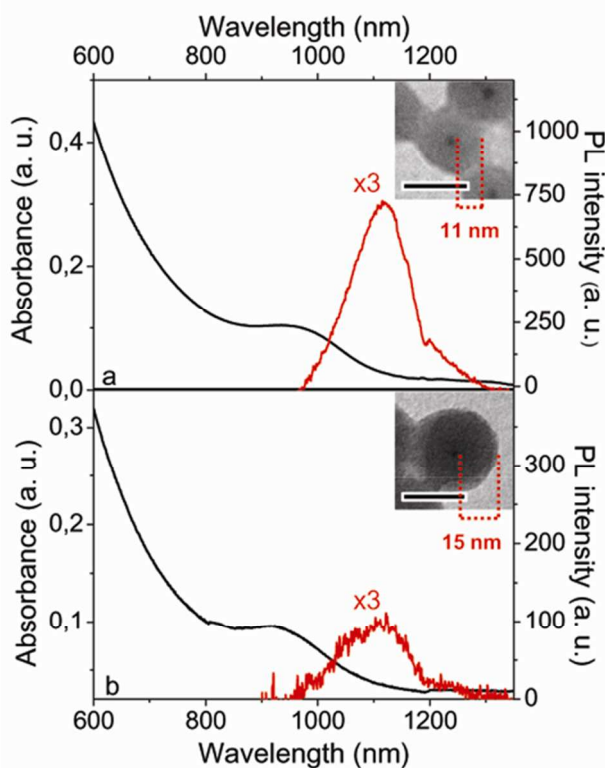


**Figure 5.** Vis-NIR absorption and PL emission spectra ( $\lambda_{\text{exc}}=700$  nm) of PbS@SiO<sub>2</sub> NPs in ethanol solution, for TEOS volume of 30  $\mu\text{L}$  (a) and 80  $\mu\text{L}$  (b), respectively, with the corresponding TEM micrograph (scale bar = 25 nm).

The optical characterization of PbS@SiO<sub>2</sub> NPs, with the silica shell thickness of 11 nm and 15 nm has been reported in Figure 5a and 5b, respectively. The vis-NIR absorption spectrum of PbS@SiO<sub>2</sub> NPs, with the silica shell thickness of 11 nm shows the presence of a shoulder, instead of the well-defined excitonic peak which is peculiar of PbS NCs (Figure 2) before the incorporation in the silica matrix (Figure 5a). Similarly, in the case of PbS@SiO<sub>2</sub> NPs with the silica shell 15 nm thick, an analogous shoulder can be observed (Figure 5b). Remarkably, the emission of PbS NCs after their incorporation in the silica bead, is retained, as displayed in Figure 5a and 5b. Namely, a PL peak of PbS@SiO<sub>2</sub> NPs is detected at 1115 nm and 1122 nm for thickness of the silica shell is equal to 11 nm and 15 nm, respectively, thus indicating in both cases, a slight blue shift, with respect to PbS NC emission in toluene solution. An analogous blue-shift was previously observed also for CdTe NCs coated with a silica shell, obtained by using APS as silanoic precursor instead of TEOS.<sup>36</sup> For those particles,

Schrödter and coworkers attributed the blue-shift to a degradation process due to the ligand exchange. In our case, besides the pristine capping molecules removal, with their concomitant replacement with TEOS, the presence of hydrolysed TEOS molecules can be thought to induce an oxidation of PbS NC surface. In fact, it is well known that PbS NCs are inclined to oxidation when handled in air, like in our case. Therefore, the formation of a very thin layer of oxide on PbS NC surface, reducing the actual size of the core, can account for the PL peak blue-shift. For both samples, a shoulder at longer wavelength side of the PL emission peak can be observed. Such a feature could be ascribed to some possible impurities present at the surface and/or, to the presence of a small fraction of multicore PbS@SiO<sub>2</sub> NPs, whose formation cannot be totally excluded also in the samples with the narrower size distribution, and emitting at higher wavelength. In addition, a comparison of the PL spectra of the two samples with different silica shell thicknesses, shows a not negligible emission quenching for the 15 nm thick silica shell sample. Considering that the starting PbS NC concentration is the same in the two cases, as can be also inferred by the comparable intensity of the absorption signal (Figure 5a), the PbS@SiO<sub>2</sub> NPs with the thinner shell present a more intense emission. Such a difference in the PL intensity can be ascribed to a more effective scattering of the emitted radiation across the thicker silica shell.

#### Functionalization of PbS@SiO<sub>2</sub> nanoparticles with primary amine groups

Primary amine groups have been introduced on the silanized surface of PbS NCs, by reaction with APS in alcoholic solution. The PbS@SiO<sub>2</sub> NPs with 11 nm thick silica shell and with a higher PL intensity have been selected and used for the functionalization process. The successful functionalization has been assessed by qualitative investigating presence of amine groups at the surface of the APS-functionalized PbS silica coated NPs, by means of reaction with ninhydrin, which induced the formation of Ruhemann's purple, blue coloured and then easily detectable (Figure S3, Supporting Information).

#### Bioconjugation of NIR-emitting PbS@SiO<sub>2</sub> nanoparticles

The viability of bioconjugation routes on the prepared PbS@SiO<sub>2</sub> has been assessed by means of functionalization of the nanostructures with biotin, a relevant molecule in biochemistry and biomedicine.

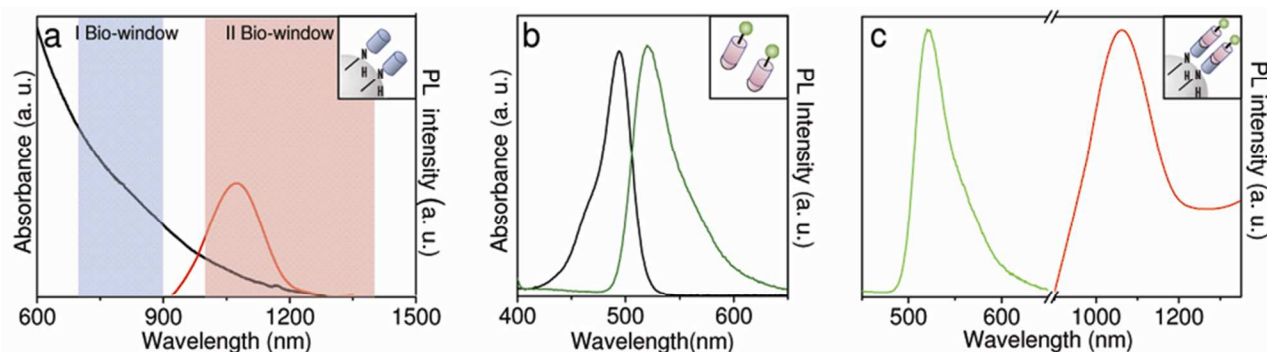


**Figure 6.** (a) Vis-NIR absorption and PL emission spectra ( $\lambda_{\text{exc}}=700$  nm) of biotinylated PbS@SiO<sub>2</sub> NPs in bicarbonate buffer (25 mM, pH=9.5). (b) Vis-NIR absorption and PL ( $\lambda_{\text{exc}}=450$  nm) spectra of FITC-modified streptavidin in carbonate buffer solution (pH=9.5). (c) PL spectrum of biotinylated PbS@SiO<sub>2</sub> NPs after the molecular recognition with the FITC-modified streptavidin in the vis ( $\lambda_{\text{exc}}=450$  nm, green line) and NIR ( $\lambda_{\text{exc}}=700$  nm, red line) range.

The reaction between primary amine groups  $-\text{NH}_2$  grafted on PbS@SiO<sub>2</sub> NP surface and a biotin activate ester has been promoted. The biotinylation procedure and the successive bioconjugation reaction with streptavidin have been carried out accordingly to the procedure reported by Ye et al.,<sup>26</sup> with slight modifications. In particular, a biotinylation reaction has been induced between N-Hydroxysuccinimidobiotin and amine-functionalized PbS@SiO<sub>2</sub> NPs in a mixture of H<sub>2</sub>O/DMSO (1:1). The solubility of amine-functionalized PbS@SiO<sub>2</sub> NPs in DMSO is rather low, as demonstrated by the slight turbidity of the solution at the beginning of the reaction, being the DMSO in excess with respect to water. However, with the progress of the reaction, the solution gradually turns limpid, indicating that the NP surface is changing. After purification, biotinylated PbS@SiO<sub>2</sub> NPs have been dissolved in sodium bicarbonate buffer (25 mM, pH=9.5). The vis-NIR absorption investigation clearly reveals the lack of the excitonic features of biotinylated silica coated PbS NCs, probably due to the different dielectric properties of the aqueous environment surrounding the NPs (Figure 6a, black line). Moreover, the PbS@SiO<sub>2</sub> NP conjugation with biotin molecules has been carried out exploiting a lower NP concentration range, which can be thought to generate a shoulder in the UV-Vis absorption spectrum instead of a well-defined peak. Similar observations were extensively documented in literature for aqueous-synthesized PbS NCs.<sup>37</sup> Interestingly, the emission properties of biotinylated silica coated NPs are retained, although a slight blue shift of about 42 nm with respect the emission in the PL spectrum of starting PbS@SiO<sub>2</sub> NPs can be clearly observed (Figure 6a, red line). This phenomenon can be explained taking into account that the biotinylated silica coated NPs are dispersed in alkaline aqueous buffer (sodium bicarbonate buffer, pH 9.5), therefore the blue shift of emission, recorded in their PL spectrum, can be ascribed to structural changes occurring at the PbS NC surface, due to the crosslinking of hydroxyl ions through the silica matrix. It is reasonable to assume that an oxidation process may occur at the NC surface, as suggested by spectroscopic studies on pH-dependent changes in PL of CdTe NCs, that demonstrated how a partial removal of

ions from the NC surface, degrading it, can result in a blue shift of the emission maximum.<sup>38-40</sup>

Interestingly, the feature detected at longer wavelength side of the PL signal in the spectrum of PbS@SiO<sub>2</sub> NPs, are not present in the PL spectrum of the biotinylated sample, probably due to the intensive and iterated purification procedure carried out upon the biotinylation reaction. Finally, a molecular recognition test between biotin and FITC-labeled avidin, characterized by a remarkable selectivity and specificity has been carried out.<sup>41</sup> In particular, the presence of a FITC green-emitting moiety in the protein structure allows to assess the effective binding between the avidin and biotin and, thus, the ultimate biotinylation of amine-functionalized PbS@SiO<sub>2</sub> NPs. In Figure 6b the optical characterization of FITC-labeled streptavidin, in sodium bicarbonate buffer, is reported. An absorption peak at 494 nm and an emission signal at 520 nm have been detected. These optical features are unambiguously ascribable to the FITC green emitting moiety. Figure 6c shows the optical characterization in the visible (green line) and NIR (red line) spectral range of biotinylated silica coated PbS NPs after streptavidin binding.

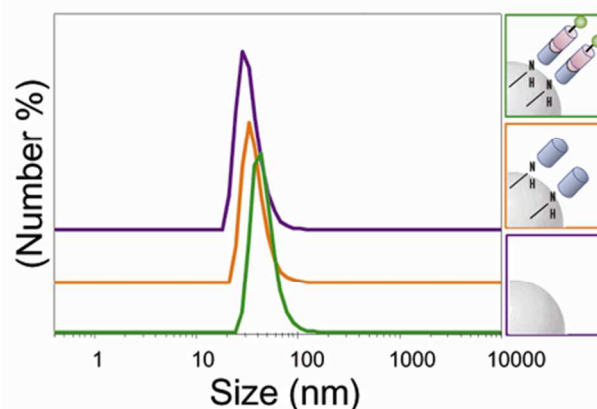


**Figure 7.** Hydrodynamic diameters distribution by number of (a) PbS@SiO<sub>2</sub> NPs (purple line) (b) biotinylated PbS@SiO<sub>2</sub> NPs (orange line) and (c) biotinylated PbS@SiO<sub>2</sub> NPs functionalized with streptavidin-FITC (green line).

In the visible range, the observed emission peak at 520 nm can be attributed to the streptavidin-FITC, thus clearly confirming the streptavidin-FITC recognition event on the biotin decorated PbS@SiO<sub>2</sub> NPs and, therefore the occurrence of biotinylation process. Interestingly, the PL emission peak in the NIR region, at 1062 nm, is retained. The further blue shift observed with respect to the biotinylated silica coated NPs can be explained by a slight reduction of the PbS NC cores occurring upon the bioconjugation reaction. Indeed, as previously reported, during biotinylation, in the alkaline buffer, NPs are in extensive contact with hydroxyl groups, that are likely to diffuse into the silica network, thus further promoting the oxidation process, that results in a thickening of the oxide layer and in the concomitant reduction in size of the PbS core.<sup>38-40</sup>

The whole functionalization and bioconjugation procedure has been also monitored by DLS and  $\zeta$ -potential measurements to further assess the evolution in size of the system under study. The DLS analysis has revealed the occurrence of a monomodal and very homogeneous population in all of the investigated samples (Table S1 and Figure 7). In particular, for the starting silica coated PbS NPs the average hydrodynamic diameter ( $D_H$ ) has resulted of about 36 nm, hence slightly larger than the 27 nm, measured by TEM. However the recorded higher  $D_H$  value can be reasonably accounted for by the presence of a hydration shell at the PbS@SiO<sub>2</sub> NP surface. Interestingly  $D_H$  values obtained for the biotinylated PbS@SiO<sub>2</sub> NPs and the relative streptavidin-bioconjugated NPs have resulted of 41 nm and 48 nm, respectively, thus confirming the occurrence of both biotinylation and subsequent molecular recognition reaction. Remarkably, the  $\zeta$ -potential values measured for silica coated PbS NPs and biotinylated PbS@SiO<sub>2</sub> NPs, before and after streptavidin recognition reaction, have been found -29.5 mV, -22.7 mV and -28.4 mV, respectively, thus indicating a good colloidal stability of the investigated NPs all along the functionalization process.

## Conclusions

The synthesis of a silica shell on hydrophobic, NIR emitting PbS NCs, by means of a water-in-oil reverse microemulsion approach, has been here reported. The influence of the experimental parameters, namely PbS NC, ammonia and TEOS concentration on the resulting NPs has been investigated by means of vis-NIR absorption and photoluminescence spectroscopy, and transmission electron microscopy and their specific role discussed in terms on their influence on the final morphology and optical properties of the obtained silica coated nanostructures. The specific conditions for achieving very homogeneous and spherical PbS@SiO<sub>2</sub> NPs, with one particle for each silica bead, have been carefully defined. Interestingly, the silica coated nanostructures have been demonstrated to preserve the optical absorption and, even more importantly, the emission properties. The PbS@SiO<sub>2</sub> NPs with 11 nm thick silica shell, exhibiting the highest PL intensity, have been selected for the bioconjugation with a standard biotinylation reaction. The molecular recognition of the bioconjugated

nanostructures with a FITC-labelled streptavidin has finally confirmed the success of the biofunctionalization on PbS@SiO<sub>2</sub> NP surface. DLS and  $\zeta$ -potential measurements have provided a prompt tool to monitor the functionalization steps and, most importantly, have shown a high colloidal stability of the NPs before and after bioconjugation. The obtained biotin decorated PbS@SiO<sub>2</sub> NPs have been verified to retain the emission properties of the pristine PbS NCs, thus resulting extremely valuable functional materials to be promptly integrated in biologically relevant structures. The investigated bioconjugated nanosystems are very promising candidates as specific tumour cell targeting for real in vivo bio-imaging, particularly appealing as fluorescent nanoprobe in the 'second biological window', for tumour diagnostic, as the size and shape of these agents can be also finely adjusted to modulate pharmacokinetics and biodistribution.

## Acknowledgements

This work was partially supported by the Italian National Consortium for Material Science and Technology (INSTM) and by MAAT PON project (CUPB31C12001230005, "Molecular Nano-technology for Health and Environment"). The authors gratefully acknowledge Dr. A. Falqui for HRTEM measurements.

## Notes and references

<sup>a</sup> Dipartimento di Chimica, Università degli Studi di Bari, Via Orabona 4, I-70126, Bari, Italy.

<sup>b</sup> CNR-IPCF c/o Dipartimento di Chimica, Università degli Studi di Bari, Via Orabona 4, I-70125, Bari, Italy. \* Tel.: +39 (0)80 5442027. E-mail: lucia.curri@ba.ipcf.cnr.it.

<sup>c</sup> Dipartimento di Farmacia - Scienze del farmaco, Università degli Studi di Bari, Via Orabona 4, I-70126, Bari, Italy.

‡These authors contributed equally.

Electronic Supplementary Information (ESI) available: Size statistical analysis of silanized PbS NPs, TLC plate showing the ninhydrin test results and a table summarizing the  $D_H$  and  $\zeta$ -potential values for the investigated samples.- See DOI: 10.1039/b000000x/

- 1 A. M. Smith, M. C. Mancini and S. Nie, *Nat. Nanotechnol.*, 2009, **4**, 710.
- 2 K. Welsher, S. P. Sherlock and H. Da, *Proc. Natl. Acad. Sci. U. S. A.*, 2011, **108**, 8943.
- 3 M.-F. Tsai, S.-H. G. Chang, F.-Y. Cheng, V. Shanmugam, Y.-S. Cheng, C.-H. Su and C.-S. Yeh, *ACS Nano*, 2013, **7**, 5330.
- 4 N. Won, S. Jeong, K. Kim, J. Kwag, J. Park, S. G. Kim and S. Kim, *Molecular Imaging*, 2012, **11**, 338.
- 5 D. J. Naczynski, M. C. Tan, M. Zevon, B. Wall, J. Kohl, A. Kulesa, S. Chen, C. M. Roth, R. E. Riman and P. V. Moghe, *Nat. Commun.*, 2013, **4**, 2199.
- 6 H.-T. Sun, J. Yang, M. Fujii, Y. Sakka, Y. Zhu, T. Asahara, N. Shirahata, M. Ii, Z. Bai, J.-G. Li and H. Gao, *Small*, 2011, **2**, 199.
- 7 I. L. Medintz, H. T. Uyeda, E. R. Goldman and H. Mattoussi, *Nature Mater.*, 2005, **4**, 435.

- 8 M. W. Ambrogio, C. R. Thomas, Y.-L. Zhao, J. I. Zink and J. F. Stoddart, *Acc. Chem. Res.*, 2011, **44**, 903.
- 9 Z. Li, J. C. Barnes, A. Bosoy, J. F. Stoddart and J. I. Zink, *Chem. Soc. Rev.*, 2012, **41**, 2590.
- 10 L. Wang, W. Zhao and W. Tan, *Nano Res.*, 2008, **1**, 115.
- 11 M. S. Bakshi, P. Thakur, G. Kaur, H. Kaur, T. S. Banipal, F. Possmayer and N. O. Petersen, *Adv. Func. Mater.*, 2009, **19**, 1451.
- 12 S. Zhang, P. W. Cyr, S. A. Mc Donald, G. Konstantatos and E. H. Sargent, *Appl. Phys. Lett.*, 2005, **87**, 233101.
- 13 D. M. N. M. Dissanayake, R. A. Hatton, T. Lutz, C. E. Giusca, R. J. Curry and S. R. P. Silva, *Appl. Phys. Lett.*, 2007, **91**, 133506.
- 14 K. N. Bourdakos, D. M. N. M. Dissanayake, T. Lutz, S. R. P. Silva and R. J. Curry, *Appl. Phys. Lett.*, 2008, **92**, 153311.
- 15 M. Corricelli, F. Enrichi, D. Altamura, L. De Caro, C. Giannini, A. Falqui, A. Agostiano, M. L. Curri and M. Striccoli, *J. Phys. Chem. C*, 2012, **116**, 6143.
- 16 E. H. Sargent, *Adv. Mater.* 2005, **17**, 515.
- 17 L. Levina, V. Sukhovatkin, S. Musikhin, S. Cauchi, R. Nisman, D.P. Bazett-Jones and E. H. Sargent, *Adv. Mater.*, 2005, **17**, 1854.
- 18 D. Wang, J. Qian, F. Cai, S. He, S. Han and Y. Mu, *Nanotechnology*, 2012, **23**, 245701.
- 19 R. Hu, W.-C. Law, G. Lin, L. Ye, J. Liu, J. Liu, J. L. Reynolds and K.-T. Yong, *Theranostics*, 2012, **2**, 723.
- 20 D. Wang, J. Qian, F. Cai, S. He, S. Han and Y. Mu, *Nanotechnology*, 2012, **23**, 245701.
- 21 W. Yang, Y. Cheng, T. Xu, X. Wang and L.-P. Wen, *Eur. J. Med. Chem.*, 2009, **44**, 862.
- 22 M. Li, J. W. Y. Lam, F. Mahtab, S. Chen, W. Zhang, Y. Hong, J. Xiong, Q. Zheng and B. Z. Tang, *J. Mater. Chem. B*, 2013, **1**, 676.
- 23 M. Corricelli, D. Altamura, L. De Caro, A. Guagliardi, A. Falqui, A. Genovese, A. Agostiano, C. Giannini, M. Striccoli and M. L. Curri, *CrystEngComm*, 2011, **13**, 3988.
- 24 Y. Han, J. Jiang, S. Seong-Lee and J. Y. Ying, *Langmuir*, 2008, **24**, 5842.
- 25 E. Fanizza, N. Depalo, L. Clary, A. Agostiano, M. Striccoli and M. L. Curri, *Nanoscale*, 2013, **5**, 3272.
- 26 L. Ye, R. Pelton, M. A. Brook, *Langmuir*, 2007, **23**, 5630.
- 27 M. Darbandi, W. Lu, J. Fang, T. Nann, *Langmuir*, 2006, **22**, 4371.
- 28 H. L. Ding, Y. X. Zhang, S. Wang, J. M. Xu, S. C. Xu and G. H. Li, *Chem. Mat.*, 2012, **24**, 4572.
- 29 F. J. Arriagada and K. J. Osseo-Asare, *J. Colloid Interf. Sci.*, 1999, **211**, 210.
- 30 E. E. Fenn, D. B. Wong, C. H. Giammarco and M. D. Fayer, *J. Phys. Chem. B*, 2011, **115**, 11658.
- 31 T. T. Tan, S. T. Selvan, L. Zhao, S. Gao and J. Y. Ying, *Chem. Mater.*, 2007, **19**, 3112.
- 32 M. P. Pileni, T. Zemb and C. Petit, *Chem. Phys. Lett.*, 1985, **118**, 414.
- 33 M. P. Pileni, *Nat. Mater.*, 2003, **2**, 145.
- 34 V. K. LaMer and R. H. Dinegar, *J. Am. Chem. Soc.*, 1950, **72**, 4847.
- 35 Y. Huang and J. E. Pemberton, *Colloids Surf., A*, 2010, **360**, 175.
- 36 A. Schroedter, H. Weller, R. Eritja, W. E. Ford and J. M. Wessels, *Nano Lett.*, 2002, **2**, 1363.
- 37 L. Levina, V. Sukhovatkin, S. Musikhin, S. Cauchi, R. Nisman, D. P. Bazett-Jones and E. H. Sargent, *Adv. Mater.*, 2005, **17**, 1854.
- 38 H. Zhang, Z. Zhou, B. Yang and M. Gao, *J. Phys. Chem. B*, 2003, **107**, 8.
- 39 K. Boldt, O. T. Bruns, N. Gaponik, A. Eychmüller, *J. Phys. Chem. B*, 2006, **110**, 1959.
- 40 M. Gao, S. Kirstein, H. Möhwald, A. Rogach, A. Kornowski, A. Eychmüller and H. Weller, *J. Phys. Chem. B*, 1998, **102**, 8360.
- 41 S. M. Saleh, A. Reham, T. Hirsch, O. S. Wolfbeis, *J. Nanopart. Res.*, 2011, **13**, 4603.